Chemical Science

EDGE ARTICLE

View Article Online
View Journal | View Issue

Cite this: *Chem. Sci.*, 2015, **6**, 5531

Water splitting with polyoxometalate-treated photoanodes: enhancing performance through sensitizer design†

John Fielden,‡*[ab] Jordan M. Sumliner,[a] Nannan Han,[a] Yurii V. Geletii,[a] Xu Xiang,[ac] Djamaladdin G. Musaev,*[a] Tianquan Lian*[a] and Craig L. Hill*[a]

Visible light driven water oxidation has been demonstrated at near-neutral pH using photoanodes based on nanoporous films of TiO_2, polyoxometalate (POM) water oxidation catalyst $[\{Ru_4O_4(OH)_2(H_2O)_4\}(\gamma\text{-}SiW_{10}O_{36})_2]^{10-}$ (**1**), and both known photosensitizer $[Ru(bpy)_2(H_4dpbpy)]^{2+}$ (**P2**) and the novel crown ether functionalized dye $[Ru(5\text{-crownphen})_2(H_2dpbpy)]$(**$H_2$2**). Both triads, containing catalyst **1**, and catalyst-free dyads, produce O_2 with high faradaic efficiencies (80 to 94%), but presence of catalyst enhances quantum yield by up to 190% (maximum 0.39%). New sensitizer **$H_2$2** absorbs light more strongly than **P2**, and increases O_2 quantum yields by up to 270%. TiO_2-**2** based photoelectrodes are also more stable to desorption of active species than TiO_2–**P2**: losses of catalyst **1** are halved when pH > TiO_2 point-of-zero charge (pzc), and losses of sensitizer reduced below the pzc (no catalyst is lost when pH < pzc). For the triads, quantum yields of O_2 are higher at pH 5.8 than at pH 7.2, opposing the trend observed for **1** under homogeneous conditions. This is ascribed to lower stability of the dye oxidized states at higher pH, and less efficient electron transfer to TiO_2, and is also consistent with the 4th **1**-to-dye electron transfer limiting performance rather than catalyst TOF_{max}. Transient absorption reveals that TiO_2–**2–1** has similar 1st electron transfer dynamics to TiO_2–**P2–1**, with rapid (ps timescale) formation of long-lived $TiO_2(e^-)$–**2–1**(h^+) charge separated states, and demonstrates that metallation of the crown ether groups (Na^+/Mg^{2+}) has little or no effect on electron transfer from **1** to **2**. The most widely relevant findings of this study are therefore: (i) increased dye extinction coefficients and binding stability significantly improve performance in dye-sensitized water splitting systems; (ii) binding of POMs to electrode surfaces can be stabilized through use of recognition groups; (iii) the optimal homogeneous and TiO_2-bound operating pHs of a catalyst may not be the same; and (iv) dye-sensitized TiO_2 can oxidize water without a catalyst.

Received 20th April 2015
Accepted 10th June 2015

DOI: 10.1039/c5sc01439e

www.rsc.org/chemicalscience

Introduction

Efficient water oxidation remains a key challenge in the development of systems for artificial photosynthesis. The last five years have witnessed dramatic progress in water oxidation catalyst (WOC) speed and stability,[1,2] with leading catalysts now showing turnover frequencies (TOFs) comparable to that of the biological OEC.[1r,2j] Even so, efforts to develop complete devices for efficient solar fuel production are still in their infancy.[3] Any such system is likely to be centred on a water-oxidizing photoelectrode that serves as a man-made analogue of nature's light-driven water splitting agent, photosystem II.

Prior to development of the dye-sensitized solar cell (DSSC), dye sensitized TiO_2 (ds-TiO_2) was pioneered as a material for light-driven water oxidation.[4] Many ruthenium-based dyes have, in their Ru^{3+} oxidation state, sufficient potential to oxidize water and thanks to two decades of research into DSSCs, efficient, mesoporous TiO_2 photoelectrodes are easily accessible.[5,6] Consequently, incorporation of WOCs into ds-TiO_2 has become an important approach to water-oxidizing photoanodes.[7] Although many of these devices are hampered by inefficient electron transfer (ET),[7a,d] or insufficient catalyst speed,[7i] single-wavelength quantum efficiencies as high as 14% were recently reported with a fast ruthenium polypyridyl-based catalyst.[7j] Successful engineering of practical devices will require not only

[a]*Department of Chemistry, Cherry L. Emerson Center for Scientific Computation, Emory University, Atlanta, GA 30322, USA. E-mail: chill@emory.edu*

[b]*WestCHEM, School of Chemistry, University of Glasgow, G12 8QQ, UK*

[c]*State Key Laboratory of Chemical Resource Engineering, Beijing University of Chemical Technology, Beijing 1000029, P. R. China*

† Electronic supplementary information (ESI) available: Details of materials, synthetic procedures, crystallographic data; details of ultrafast and nanosecond transient absorption spectrometers and photoelectrochemistry set-up; supporting UV-vis, cyclic voltammetry and transient absorption measurements. CCDC 1059343. For ESI and crystallographic data in CIF or other electronic format see DOI: 10.1039/c5sc01439e

‡ Current address: School of Chemistry, University of East Anglia, Norwich, NR4 7TJ, UK. John.Fielden@uea.ac.uk

fast stable WOCs, efficient stable sensitizers, and rapid, directional ET from the WOC to the oxidized sensitizer, but also sensitizer and catalyst binding that resists aqueous buffers and electrolytes. Even so, there has been little work addressing the influence of sensitizers on performance: Meyer *et al.* have developed strategies to mitigate dye desorption,[7k,8] and covalent linkages have been engineered between Ru tris-bipyridyls and water oxidation catalysts,[7a,d,g,h,l] but to our knowledge there are no systematic studies into the effect of light absorption and catalyst binding properties.

We, and other groups, are investigating the incorporation of polyoxometalate (POM) based WOCs into dye-sensitized TiO_2,[7i,9] and their deposition onto other electrode surfaces.[10] These oxidatively stable, molecular all-inorganic WOCs can achieve efficient, fast homogeneous light driven water oxidation using $[Ru(bpy)_3]^{2+}$ as photosensitizer, but turnover numbers (TONs) are limited by degradation of dye.[2,11] As oxidative degradation of Ru-polypyridyls occurs primarily through attack of hydroxide and hydroxyl radicals on the oxidized, Ru^{3+} state,[12] placing the dye and catalyst on a surface (*e.g.* TiO_2) can be expected to mitigate degradation. Close association on the surface should speed ET from catalyst-to-dye, reducing time spent by the dye in the vulnerable Ru^{3+} state, and also reduce exposure of the dye to nucleophilic species. Recently, we found that *vs.* solution, ET from the catalyst $[\{Ru_4O_4(OH)_2(H_2O)_4\}(\gamma\text{-}SiW_{10}O_{36})_2]^{10-}$ (**1**) to the oxidized state of the $[Ru(bpy)_2(H_4dpbpy)]^{2+}$ (**P2**) dye is dramatically accelerated on TiO_2 and SnO_2, and that long-lived charge separated states are generated.[7i,9b] Furthermore, enhancement of visible-light photocurrents by **1** suggested water oxidation. However, this was not confirmed, and rapid losses of active species occurred under turnover conditions – an increasingly recognized problem in ds-TiO_2 based water splitting.[7k,8] POM-based catalysts present a particular challenge, as catalytically useful, transition metal substituted POMs such as **1** cannot be derivatized through the strategies used for other POM anions,[13] and their terminal W=O groups are both poor hydrogen bond acceptors and very weak ligands. Consequently, binding predominantly depends on size and surface charge.

In this study, our focus moves from ET dynamics, to quantifying photoelectrochemical water oxidation by **1** at ds-TiO_2 photoanodes based both on **P2**, and new, crown ether decorated dye $[Ru(5\text{-crownphen})_2(H_2dpbpy)]$(**$H_2$2**, Fig. 1) under visible light. While both systems show high (80–90%) faradaic efficiency, **$H_2$2** increases maximum quantum yields almost 4×, while also dramatically reducing the loss of **1** when pH > TiO_2 pzc. This provides the first clear demonstration that major performance gains can be achieved through sensitizer design, that non-covalent recognition groups can stabilize binding of POMs at surfaces, and also facilitates an in-depth understanding that may guide further studies of POM-based photoelectrodes. In addition, we quantify water oxidation by catalyst-free ds-TiO_2 for the first time, finding a high faradaic efficiency, and low but appreciable quantum yield for this under-recognized phenomenon.

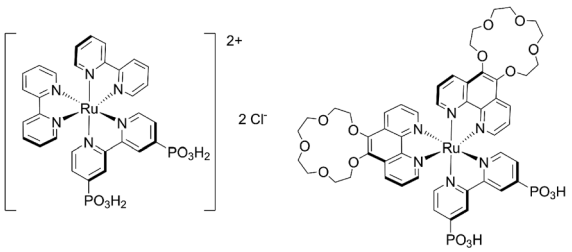

P2 **$H_2$2**

Fig. 1 Molecular structures of **P2**, isolated as its chloride salt, and **2**, obtained in its doubly deprotonated, neutral form **$H_2$2**.

Results and discussion

Sensitizer design, synthesis and structure

The design of **$H_2$2** was inspired by previous reports of 5-crown phenanthroline derivatized Ru-polypyridyl sensitizers and rhenium carbonyls.[14,15] The Ru-based systems[14] bind alkali and alkaline earth metals, but retain very similar photophysical and redox properties to underivatized $[Ru(bpy)_3]^{2+}$, $[Ru(bpy)_2(phen)]^{2+}$ and $[Ru(bpy)(phen)_2]^{2+}$, while [(5-crown-phen)$Re(CO)_3Cl$] has shown an ability to associate with $[PW_{12}O_{40}]^{3-}$ in solid state and solution.[15] Therefore, 5-crown-phen appeared an obvious way to increase the strength of sensitizer–catalyst interactions, while retaining similar photophysical and redox properties to **P2**. In addition, phenanthroline ligands increase extinction coefficients compared to bipyridines.[16]

5-crown-phen is easily accessed from phenanthroline, using established methods.[14b] Subsequently, **$H_2$2** was synthesized in moderate yields starting from this ligand and $Ru(DMSO)_4Cl_2$, using methods described in the ESI (Scheme S1†). **$H_2$2**'s molecular structure and purity has been confirmed by ^{1}H-NMR, ESI$^+$-MS, elemental analysis and X-ray crystallography. A thermal ellipsoid plot of its crystal structure (space group *Pnna*) is displayed in Fig. 2 (excluding crystallographically located water and acetone); selected bond lengths and angles can be found in Table S1 (ESI†). The coordination geometry of the *pseudo*-octahedral ruthenium atom is very similar to that observed in $[Ru(phen)_2(bpy)]^{2+}$,[16] with distortion resulting from

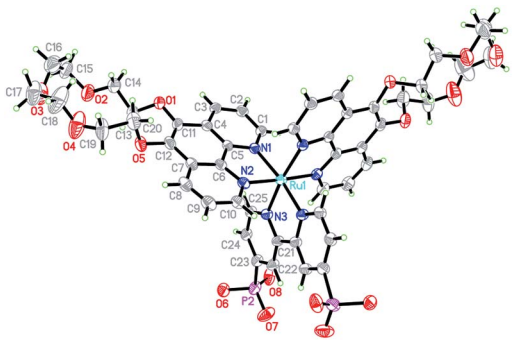

Fig. 2 Representation of the molecular structure of **$H_2$2** (30% probability ellipsoids). Symmetry equivalent atoms are unlabelled. C atoms are grey; N, blue; O, red; P, magenta; Ru, light blue; H, green circles of arbitrary radii.

the small bite angles (*ca.* 80°) of the ligands. Notably, the presence of $-PO_3H$ groups, crown ethers and water molecules leads to a 3D hydrogen bonded network based on chains of $\mathbf{Et_2}$**2** molecules linked *via* $-PO_3H$ (Fig. S1, ESI†).

Electronic spectroscopy, cyclic voltammetry and DFT calculations: the effect of cations on 2

The new sensitizer $\mathbf{H_2}$**2** has a similar UV-vis spectrum to **P2** in water (Fig. 3), but with higher extinction coefficients for both ligand centred and MLCT transitions. This is consistent with typical observations for phenanthroline,[16] *vs.* bipyridine complexes and results from the larger π-conjugated system. The aqueous electrochemistry of the two sensitizers is also very similar, with $\mathbf{H_2}$**2** showing a *pseudo*-reversible Ru^{2+}/Ru^{3+} couple at +1.35 V *vs.* Ag/AgCl. Ligand reductions, however are obscured by the onset of proton reduction in aqueous media.

Alkali and alkaline earth metal cations bind strongly to *mono*-5-crown-phen and 5-crown-dppz ruthenium complexes in MeCN, but have only small effects on the spectral and electrochemical properties.[14] While $\mathbf{H_2}$**2** is insoluble in organic media, study of the esterified precursor $[\mathbf{Et_4}\mathbf{2}][PF_6]_2$ has produced results (Table 1 and Fig. S2†) consistent with this literature. Cation binding has only a minimal influence on the photophysical properties of the bis-5-crown-phen system $[\mathbf{Et_4}\mathbf{2}]^{2+}$, with almost no change seen in the MLCT absorption, and a 1 nm red shift in ^{3}MLCT emission, upon addition of 500 equivalents of Na^+. A more significant change (*ca.* 5% fall) is observed in the intensity of the 272 nm ligand centred absorption band. Addition of the same concentration of non-binding NBu_4PF_6 had no effect on ^{3}MLCT emission and led to a 23% *increase* in the intensity of the 272 nm band, indicating that Na^+ binding and not a just simple increase in ionic strength is responsible for the change. Greater changes are seen when Mg^{2+} is added: a slight broadening and flattening of the MLCT absorption, a 7 nm red shift in ^{3}MLCT emission, and a 14% increase in the intensity of the 272 nm band. Even so, for both cations, these results imply that the energy of the MLCT excited state barely changes upon metallation.

Cyclic voltammetry (Table 2 and Fig. S3†) echoes the electronic spectra, by showing no change in the $Ru^{2+/3+}$ electrode potential upon addition of 75 equivalents of Na^+ or Mg^{2+}, but some effects on the ligand-based reductions. In the presence of Na^+, there are positive shifts of 20, 70 and 70 mV in $E_{1/2}$ for the 1st, 2nd and 3rd reductions. Addition of Mg^{2+} produces a 70 mV positive shift in the 1st reduction, while the 2nd and 3rd waves merge into an irreversible process with an E_{PC} midway between the 2nd and 3rd reduction of cation free $\mathbf{Et_4}$**2**.

Electronic structure calculations (DFT, B3LYP/{Lanl2dz(Ru) + 6-31G(d) (P, N, C, O, H)}) conducted on $\mathbf{H_4}\mathbf{2}^{2+}$ also indicate that changes upon addition of Na^+ and Mg^{2+} are small (Table 3). In both cases, the cation lowers the energy of the 5-crown-phen based LUMO+1 level (by *ca.* 0.14 eV), while raising the energy of the dpbpy based LUMO (*ca.* 0.06 eV for Na^+, 0.115 eV for Mg^{2+}). However, the lowest energy LUMO orbitals remain on the dpbpy ligand, favouring electron injection to TiO_2. In summary, electronic spectroscopy, cyclic voltammetry and DFT calculations show that $\mathbf{Et_4}\mathbf{2}/\mathbf{H_4}\mathbf{2}$ and their Na^+/Mg^{2+} complexes have similar electronic structures to **P2** in solution. This indicates a high degree of electronic isolation between the Ru-centre and metalla-crown, so that ground and excited state potentials of the **2** manifold relevant to electron injection into TiO_2, and oxidation of catalyst **1**, change only minimally upon metallation. The new sensitizer can therefore be expected to show similar behaviour to **P2** on the TiO_2 surface.

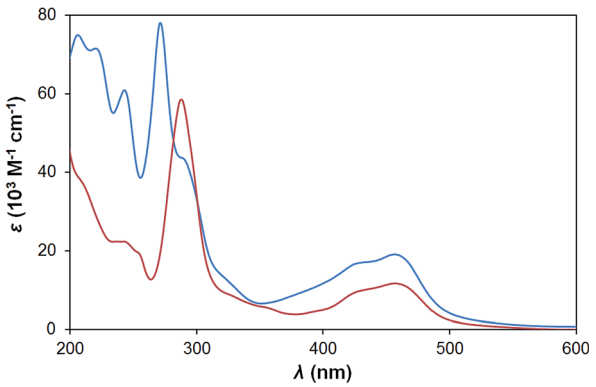

Fig. 3 UV-vis spectra of $\mathbf{H_2}$**2** (blue) and **P2** (red) in H_2O at 298 K.

Film assembly and characterization

TiO_2 films were sensitized with **P2** and **2** ($\mathbf{H_2}$**2** is assumed to deprotonate on the TiO_2 surface) in acidic conditions,[7] and where required TiO_2–**2** was metallated by soaking in solutions of $NaClO_4$ or $MgClO_4$. For photoelectrochemical (PEC) measurements, the TiO_2-dye films were treated with toluene solutions of hydrophobic $THpA_{8.5}H_{1.5}[\mathbf{1}]$ salt, as deposition of $THpA^+$ (tetraheptylammonium) at the electrode surface helps stabilize binding of **1** in aqueous buffers. For ultrafast spectroscopic studies, **1** was deposited from its tetrabutylammonium, $TBA_7H_3[\mathbf{1}]$, as this gave better transparency without introducing undesired metal cations.

Table 1 UV-visible and fluorescence data for $\mathbf{H_2}$**2** and $[\mathbf{Et_4}\mathbf{2}][PF_6]_2$ at 298 K. Concentrations *ca.* 2×10^{-5} M

Compound/solvent	Salt added	λ_{abs}/nm ($\varepsilon/10^{-4}$ M^{-1} cm^{-1})	λ_{em} (nm)
$\mathbf{H_2}$**2**/H_2O	No salt	206 (74.9), 220 (71.4), 243 (60.9), 271 (78.0), 457 (19.1)	594
$[\mathbf{Et_4}\mathbf{2}][PF_6]_2$/MeCN	No salt	207 (75.5), 245 (71.2), 272 (79.9), 380 (13.7), 449 (16.8)	635
	0.01 M $NaClO_4$	207 (75.5), 245 (70.2), 272 (76.3), 381 (13.7), 449 (16.9)	636
	0.01 M $Mg(ClO_4)_2$	206 (84.0), 246 (75.5), 272 (91.7), 379 (14.5), 449 (16.4)	642
	0.01 M NBu_4PF_6	207 (77.3), 246 (78.2), 272 (98.5), 380 (13.8), 449 (16.9)	635

Table 2 Electrochemical data for $[Et_4\mathbf{2}][PF_6]_2$ and $[H_2\mathbf{2}]$. Potentials are internally referenced to Fc/Fc+ = 0.46 V *vs.* Ag/AgCl

Compound/electrolyte	Salt added	L/L$^{-\bullet}$, $E_{1/2}/E_{PC}$, (ΔE_p, mV)	Ru$^{2+/3+}$, $E_{1/2}$, V (ΔE_p, mV)
Et_4**2**/0.1 M NBu_4PF_6 in MeCN	No salt	−0.96 (105), −1.39 (81), −1.58 (95)	1.46 (83)
	0.05 M $NaClO_4$	−0.94 (113), −1.32 (93), −1.51 (105)	1.46 (95)
	0.05 M $Mg(ClO_4)_2$	−0.891 (130), −1.501	1.46 (116)
H_2**2**/0.1 M $HClO_4$ in MeCN/H_2O	No salt	Obscured by proton reduction	1.35 (82)
P2/0.1 M $HClO_4$ in MeCN/H_2O	No salt	Obscured by proton reduction	1.34 (80)

Table 3 Calculated (B3LYP/{Lanl2dz + 6-31G(d)}) energy gaps (ΔE/eV) in **P2**, H_4**2**, H_4**2**–Na_2 and H_4**2**–Mg_2. The lowest LUMO levels are highlighted in bold

		$\Delta E_{[HOMO-Ru\ -\ LUMO+x]}$[b]	
Molecule	ΔE_{S-T}[a]	LUMO (dpbpy)	LUMO (crown/bpy)
$[Ru(bpy)_2(dpbpy)]^{2+}$ (**P2**)	2.000	**3.324**	3.712
$[Ru(5\text{-crown-phen})_2(dpbpy)]^{2+}$ (H_4**2**)	2.051	**3.367**	3.731
$[Ru(Na\text{-}5\text{-crown-phen})_2(dpbpy)]^{4+}$ (H_4**2**–Na_2)	2.111	**3.503**	3.663
$[Ru(Mg\text{-}5\text{-crown-phen})_2(dpbpy)]^{4+}$ (H_4**2**–Mg_2)	2.190	**3.510**	3.616

[a] Separation between ground state singlet and triplet excited state. [b] Separation between ruthenium based HOMO and LUMO of relevant ligand.

In our previous work,[7i] loadings of **1** were seen to depend upon the point-of-zero charge (pzc), and hence the surface positive charge, of the metal oxides TiO_2, SnO_2 and ZrO_2. Charge introduced the dye appeared to have less influence. This is confirmed in our current study. Loadings of catalyst used for PEC experiments, estimated by UV-vis (ESI, Fig. S4/Table S2†), are typically in the range of 10 to 14 nmol cm^{-2} with no clear dependence on the loading or metallation (charge) of dye (which varies between TiO_2 batches). Ratios of dye-to-catalyst are lower for **2** simply because loadings of **2** are generally lower, due to its greater size. Although assembly conditions (*e.g.* soaking time) were not strictly controlled, the results indicate that the charge of the dye is not a key factor in determining the loading of **1**. Films assembled under controlled conditions for desorption experiments confirm that the dye has at most a marginal influence (*vide infra*). For ultrafast photophysical measurements, we found that much higher catalyst loadings could be achieved with extended soaking times and higher concentration soaking solutions (Table S3†).

Transient absorption spectroscopy (TAS)

Infra-red transient spectroscopy. The photophysics of dye-sensitized semiconducting metal oxides are well-studied,[17] but investigation of systems incorporating WOCs[7a,d–h,i,9] and other catalysts[18] has started only recently. Among this work, we recently demonstrated that **1** accelerates the recovery of oxidized **P2** on TiO_2 and SnO_2, showing conclusively that this is due to the desired catalyst-to-sensitizer electron transfer.[7i] Here, we use **2** to investigate the effect of the nature of the dye (size, charge) and catalyst loading on this ET.

Electron injection from **2** into TiO_2, with and without **1**, has been studied by time-resolved mid-IR transient absorption (pump 515 nm, probe 5000 nm). Measurements on TiO_2–**2**, by comparison with a TiO_2–**N3** reference, indicate that near 100% of photons absorbed by **2** result in electron injection to the metal oxide (Fig. 4a).[17h] However, like other phosphonate binding dyes, **2**'s injection kinetics are substantially slower than those of carboxylate based **N3** – injection from excited **2** occurs over *ca.* 100 ps, instead of completing within 2 ps as for **N3**. This is considered a consequence of weak electronic communication across the tetrahedral phosphorus center,[17i] giving similar biphasic injection kinetics to **P2**,[7i] with an ultrafast component due to injection from the ^{1}MLCT excited state of the dye and a slower component arising from the ^{3}MLCT. In the presence of **1**, electron injection to TiO_2 still occurs in high yield from the ^{1}MLCT state of **2** (Fig. 4b), but the slower ^{3}MLCT component is significantly suppressed. This indicates that ET from excited **2** to TiO_2 is still the main quenching pathway when **1** is present, but as with **P2**, presence of the POM appears to introduce a competing deactivation mechanism for the ^{3}MLCT.

Treatment of a TiO_2–**2** photoelectrode with the colourless, less charged POM $[SiW_{12}O_{40}]^{4-}$ (**SiW_{12}**) confirms that the competing quenching pathway is electron transfer to **1**, rather

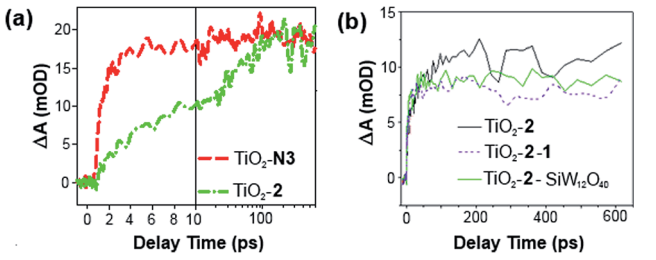

Fig. 4 Mid-IR comparison of the kinetics of electron injection in (a) TiO_2–**2** and TiO_2–**N3**, and; (b) TiO_2–**2**–**1** and TiO_2–**2**–$SiW_{12}O_{40}$. Data have been scaled to the absorbance of the supporting dyad film.

than energy transfer or an effect of its high (10^-) negative charge on the TiO_2 conduction band edge potential. This is because **SiW_{12}** produces a similar decrease in injection to TiO_2 from the ^{3}MLCT excited state (Fig. 4b), but **SiW_{12}** has no absorption bands overlapping with emission from **2**, precluding energy transfer and suggesting there must be electron transfer to this species. Interestingly, this occurs even though the W-based LUMO of SiW_{12} is significantly higher in energy than the first accessible Ru-based reduction of **1**. Similar quenching of the ^{3}MLCT excited state of $Ru(bpy)_3^{2+}$ by electron transfer to **1** has been observed in solution.[19]

Visible transient spectroscopy. Transient visible absorption measurements were performed on TiO_2–**2–1** and TiO_2–**2–M_2–1** films (M = Na^+ or Mg^{2+}), to follow electron transfer from catalyst to oxidized sensitizer. As electrons are rapidly injected into the TiO_2 conduction band, the ground state bleach observed at around 455 nm largely reflects the amount of oxidized **2**. Just as for the TiO_2–**P2** based system,[7i] addition of **1** significantly speeds the recovery of the **2** ground state bleach (Fig. 5a). Absorbance is around 65% recovered within 1 ns, and completely recovered within 100 ns, showing that electron transfer from catalyst to dye is rapid in this system. However, the half-lifetime for the ET process (*ca.* 220 ps) is slower than for TiO_2–**P2–1** (127 ps),[7i] a potential result of **2**'s increased steric bulk impeding interaction between **1** and the Ru-centre. Comparison with TiO_2–**2–SiW_{12}** confirms that the accelerated bleach recovery is a result of ET from **1** as **SiW_{12}**, which can quench excited **2** by accepting electrons but cannot transfer electrons to oxidized **2**, has only a small effect on the bleach recovery rate.

The positive charge on **2** can be increased by metallation, by 2^+ by adding Na^+, and by 4^+ with Mg^{2+}. Strong electronic interactions are observed between ion paired $Ru(bpy)_3^{2+}$ and POMs in solution,[20] so we speculated that increased charge in **2–Na_2** and **2–Mg_2** might strengthen such interactions and enhance ET from **1** to oxidized **2**. However, measurements on TiO_2–**2–1**, TiO_2–**2–Na_2–1** and TiO_2–**2–Mg_2–1** at a controlled dye-to-catalyst ratio show that this is not the case (Fig. 5b), as the kinetics of bleach recovery for the three systems are superimposable. This implies that once catalyst and dye are closely associated on the film, increasing charge on the dye does not significantly affect donor–acceptor coupling between the two species. It is also consistent with the observation that the crown and Ru-centre are electronically isolated from one another (*vide supra*), so that strengthened interaction between 5-crown-phen and **1** does not feed through to the Ru-centre. However, metallation, combined with increased soaking times and catalyst concentration has helped access triads with very high loadings of **1** (Table S3 and Fig. S5a, ESI†), confirming that bleach recovery is faster when more electron donor **1** is present.[9a] This effect saturates once there are around 1.5 catalyst molecules (**1**) per sensitizer (**2**).

Lastly, we studied the effect of pH. Compound **1** has the widest pH range of any known POM WOC (active even at pH 1),[2b] but is typically faster at pH >6.[2c] Rinsing the films in different pH solutions before measurement (Fig. S5b†), shows that at pH 1.1 bleach recovery is significantly slower than at pH 2.3 or 3.1. This suggests that increased protonation of **1** disfavours ET. However, the minimal change between pH 3.1 and 6.5 implies that either the TiO_2 film buffers the system, or factors other than the first ET are responsible for the increased speed of **1** at higher pH. This is consistent with our established mechanism for water oxidation by **1**.[2c,d]

In summary, TAS shows that the electron transfer dynamics of TiO_2–**2–1** are similar to TiO_2–**P2–1**, and that metallation of **2** does not affect **1**-to-**2** ET, but pH does. It also confirms that high loadings of **1** speed the recovery of the oxidized sensitizer, and that the main inefficiency is initial ET to **1** instead of TiO_2, which reduces the injection yield from the dye ^{3}MLCT state.

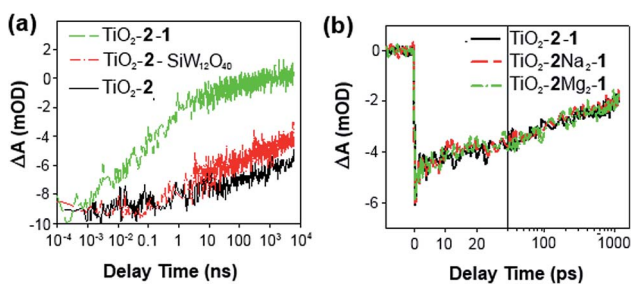

Fig. 5 (a) Ground state bleach recovery kinetics of TiO_2–**2** (black), TiO_2–**2–$SiW_{12}O_{40}$** (red) and TiO_2–**2–1**. (b) Ground state bleach recovery kinetics of TiO_2–**2–1** (black), TiO_2–**2–Na_2/1** (red) and TiO_2–**2–Mg_2–1** (green).

Photoelectrochemistry and oxygen evolution

Catalyst-free "dyads". Dye-sensitized TiO_2 and SnO_2 were first developed as materials for light-driven water oxidation in the late 1970s.[4] O_2 was not quantified, but strong arguments were presented that the observed steady-state photocurrents must be due to oxidation of water:[4c,d] the charge passed far exceeded surface coverage of dye, and $[Ru(bpy)_3]^{3+}$ had been seen to oxidize water without a catalyst under basic conditions.[12a] In our previous work with TiO_2–**P2** (pH 5.8) similar steady-state photocurrents were observed, which more than doubled in the presence of catalyst **1**. However, whether **1** was present or not, fluorescence-based O_2 probes failed to produce signals significantly above the background noise. Given the probe sensitivity and volume of electrolyte, this inability to confirm O_2 formation was entirely consistent with the charge passed during the measurements. By using a *pseudo*-Clark generator/collector set up, based upon a bipotentiostat and a platinized FTO (Pt@FTO) collector electrode,[21] we can now confirm that water is oxidized photoelectrochemically with high (80–94%) faradaic efficiency (η_F), *even in the absence of catalyst*.

Photocurrent transients for TiO_2–**P2** and TiO_2–**2** films are shown in Fig. 6. Upon illumination, both films (at pH 5.8 and 7.2) show an initial spike in generator current, resulting from electron injection to TiO_2. An instantaneous response occurs at the collector, before generator and collector currents decline towards a steady state. Photocurrent density and η_F are higher at pH 7.2 (Table 4), where water oxidation is more thermodynamically favourable, and TiO_2–**2** films show far greater photocurrents than TiO_2–**P2** (by 290% at pH 5.8, 190% at pH

7.2). Detector currents increase almost in line with photocurrents, so η_F remains high for **2**, and similar increases are seen in water oxidation internal quantum efficiency (IQE).

Despite the earlier literature, we were surprised that catalyst-free ds-TiO_2 oxidizes water. The low rate of O_2 production has made GC detection impractical, but it is difficult to envisage a source of the detector current other than reduction of O_2, based upon the following lines of evidence:

(1) There is no steady-state detector response if aqueous buffers are replaced by an acetonitrile electrolyte (Fig. S6†).

(2) Steady state detector responses are tiny (<0.1 μA) if Pt@FTO is replaced with plain FTO glass (Fig. S7†).

(3) Plain FTO glass responds strongly to injection of H_2O_2, but very weakly to air (Fig. S8†).

(4) Pt@FTO responds strongly to air (Fig. S9†).

(5) Photocurrents and faradaic efficiencies for the inorganic, and lutidine-based buffers are broadly similar.

(6) Irradiating solution-based Ru-polypyridyl dyes (Fig. S10a†) produces no detector response.

Thus, appreciable detector currents require presence of water, and do not result from Ru-dyes or organic buffer. Furthermore, the lack of response from plain FTO indicates that the detector currents do not result from H_2O_2 or other easily reduced species. Therefore, the photoelectrodes must be producing O_2, by a mechanism beyond the scope of this study – the weak (0.3 μA) response from bare TiO_2 photoanodes (Fig. S10b†) confirms that direct bandgap excitation cannot be primarily responsible. Catalysis by small Ru impurities cannot be excluded, however low levels of O_2 production are

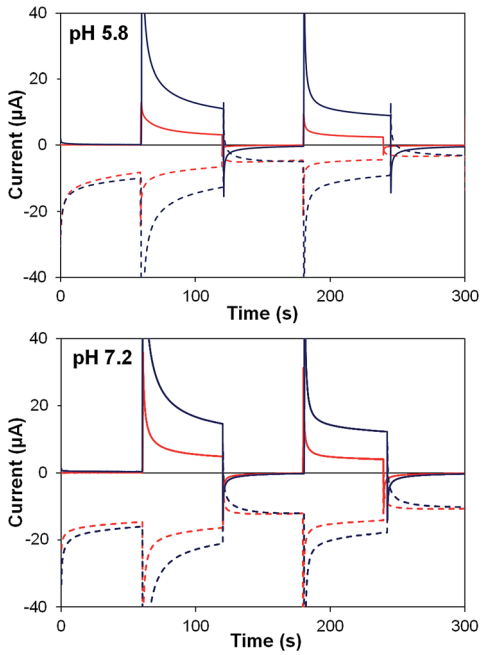

Fig. 6 Photoelectrochemical generator–collector measurements (chronoamperometry) of TiO_2–**P2** (red) and TiO_2–**2** (dark blue) at pH 5.8 and pH 7.2. Solid lines are the photoanode current; dashed lines, collector current; collector efficiency *ca.* 60%. Applied bias 0 mV *vs.* Ag/AgCl, illuminated with a 455 nm LED (33 mW cm^{-2}). Photocurrent densities are reported in Table 4.

Table 4 Photocurrents and faradaic efficiencies (η_F) for water oxidizing photoanodes based on **P2**, **2** and water oxidation catalyst **1**

	pH 5.8 Na_2SiF_6/$NaHCO_3$[a]					pH 7.2 lutidine/$HClO_4$[a]				
Photoanode	Photo-current[b], μA	Photocurrent density, μA cm^{-2}	η_F[c], %	IQE[d], %	IQE gain with **1**[e]	IQE gain for **2**[f]	Photo-current[b], μA	Photocurrent density, μA cm^{-2}	η_F[c] %	IQE[d], %	IQE gain with **1**[e]	IQE gain for **2**[f]
TiO_2–**P2**	3	5	88	0.037			4.3	7.2	94	0.058		
TiO_2–**P2**–**1**	8.5	14.2	90	0.106	186%		8.3	13.8	81	0.094	62%	
TiO_2–**2**	11.8	19.7	80	0.134		262%	12.6	21	88	0.157		170%
TiO_2–**2**Na_2–**1**	32.9	54.8	86	0.392	193%	270%	20.5	34.2	80	0.228	45%	143%

[a] $NaClO_4$ added so $[Na^+] = 200$ mM. [b] At end of first 60 s transient, average of at least two films. [c] Faradaic efficiency (η_F), average of 5 to 8 transients (≥2 films). [d] Internal quantum efficiency (IQE) for water oxidation, taking into account η_F. [e] IQE gain on addition of **1**. [f] IQE gain on replacing **P2** with **2**.

consistently observed from catalyst-free $[Ru(bpy)_3]^{2+}$ in homogeneous work,[11] and previous failure to detect O_2 from TiO_2–**P2** may be due to use of Nafion coatings.[3c] Nafion (used to segregate O_2 and H_2) has low permeability to O_2, and O_2 adheres strongly to TiO_2 surfaces.[22]

Catalyst-treated "triads". When catalyst (and Na^+ for **2**) is added to make TiO_2–**P2–1** and TiO_2–**2Na$_2$–1**, photocurrent density increases by up to 180% (Fig. 7 and 8), and new dye **2** enhances photocurrents by up to 290% *vs.* **P2**. Faradaic efficiencies remain >80% in all cases, so large increases are seen in IQE (Table 4). The biggest catalyst-driven increase in IQE (193%) occurs in TiO_2–**2** based systems at pH 5.8, and the smallest (45%) in TiO_2–**2** at pH 7.2 – consequently the advantage for **2** *vs.* **P2** (143%) is significantly smaller at pH 7.2. Photocurrent enhancement is even seen when *used* dyads (which lose >30% of their absorbance in a PEC run) are treated with **1**, eliminating film variability as a source of the increase. The results indicate that adding **1**, a known WOC, increases the rate of O_2 production by ds-TiO_2 films. In addition, higher dye extinction coefficients significantly boost activity, and are thus likely to be a good strategy to get the best out of faster WOCs. Interestingly, as we report *internal* QE this cannot simply result from more light absorption by the electrode. Instead, a higher Ru^{3+} : Ru^{2+} ratio (increased probability of excitation for each dye molecule) must increase the potential felt by the catalyst.

In extended experiments (Fig. S11–S13†) photocurrents fall below 1 μA (1.7 μA cm^{-2}) within *ca.* 3 h for TiO_2–**P2–1** at pH 5.8, 4 h for TiO_2–**2Na$_2$–1** at pH 5.8, and 5 h for TiO_2–**P2–1** at pH 7.2. For TiO_2–**2Na$_2$–1** at pH 7.2, the photocurrent is still above 1.5 μA (2.5 μA cm^{-2}) after 5 h. Stronger long term performance in the pH 7.2 buffer may be due to reduced dye desorption, however it is difficult to comment on the competing effects of stronger catalyst binding by **2**, and its reduced oxidative stability *vs.* **P2** (*vide infra*). TiO_2–**2Na$_2$–1** at pH 5.8 passed most charge, due to its high performance early in the experiment, with 0.056 C equating to 124 nmol of O_2 assuming initial η_F is maintained. This corresponds to TONs of 3 for dye **2**, and 14 for catalyst **1** after 4 hours (based on a 0.6 cm^2 active area). At pH 7.2, a similar photoelectrode passed 0.053 C after 5 h (110 nmol O_2), but due to lower loadings, $TON_{Dye} = 3$ and $TON_{Cat} = 22$. With **P2** based photoelectrodes, less than half this total charge was passed, at similar loadings of dye and catalyst. As Pt@FTO detectors degrade noticeably with use, needing cleaning after each short run,[21] we cannot confirm the quantity of O_2 produced. However, using a detector does show qualitatively that O_2 is still being produced after 5 h (Fig. S13†).

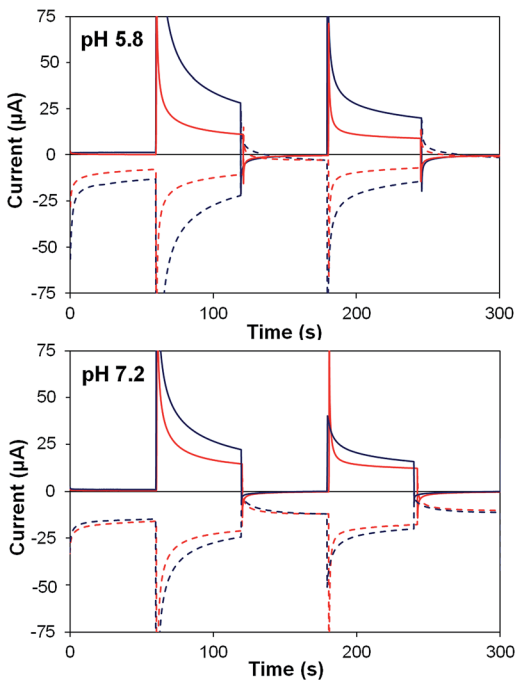

Fig. 7 Photoelectrochemical generator–collector measurements (chronoamperometry) of TiO_2–**2** (red) and TiO_2–**2Na$_2$–1** (dark blue) at pH 5.8 and pH 7.2. Solid lines are the photoanode current; dashed lines, collector current; collector efficiency *ca.* 60%. Applied bias 0 mV *vs.* Ag/AgCl, illuminated with a 455 nm LED (33 mW cm^{-2}). Photocurrent densities are reported in Table 4.

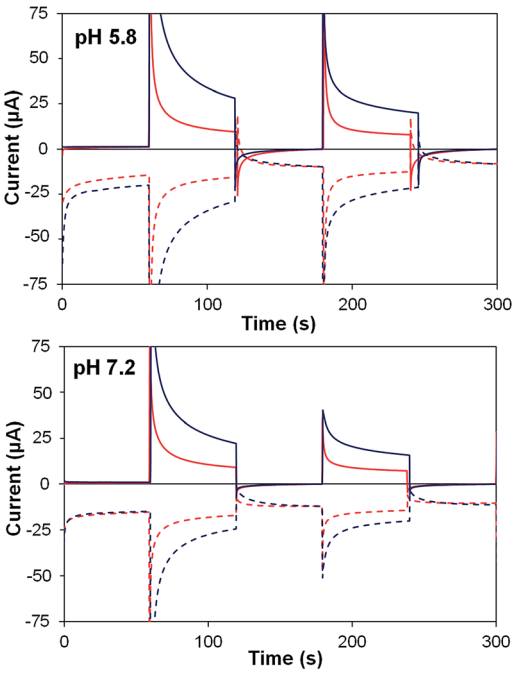

Fig. 8 Photoelectrochemical generator–collector measurements (chronoamperometry) of TiO_2–**P2–1** (red) and TiO_2–**2Na$_2$–1** (dark blue) at pH 5.8 and pH 7.2. Solid lines, photoanode current; dashed lines, collector current; collector efficiency *ca.* 60%. Applied bias 0 mV *vs.* Ag/AgCl, illuminated with a 455 nm LED (33 mW cm^{-2}). Photocurrent densities are reported in Table 5.

Analysis of the triad photocurrent data. Due to relatively high detector backgrounds, small detector currents, and film variability, detailed interpretation of η_F and photocurrent must be treated with caution. Even so, it is notable that for both dyes, gains in IQE (Table 4) upon addition of catalyst are much smaller at pH 7.2 than at pH 5.8, and that for TiO_2–**2Na$_2$–1** IQE is almost doubled at pH 5.8 compared to pH 7.2. This is despite pH 7.2 being a better operating pH for **1** in homogeneous

catalysis,[2c] and a more favourable pH for water oxidation. Three factors likely cause this behaviour: (i) higher pH raises the TiO_2 conduction band, reducing efficiency by increasing the likelihood of initial ET to catalyst **1**; (ii) Ru polypyridyls are more vulnerable to degradation at high pH, and **1** can catalyse dye degradation as well as water oxidation;[2c] and (iii) binding of **1** is weaker at high pH (*vide infra*). Evidence for (i) is seen in the smaller injection spikes observed at pH 7.2, while the more pronounced pH effect for **2** is consistent with stopped-flow observation of much faster self-degradation for this dye (*vide infra*, Fig. 9). Higher η_F for **P2** also supports the hypothesis that **2**-based photoanodes are more vulnerable to oxidative degradation – however the difference is small, suggesting dye degradation is not primarily an electrochemically mediated process. In any case, the stabilization of **2** provided by the TiO_2 surface is remarkable given the negative results obtained with $\mathbf{H_2}$**2** and related dyes in homogeneous water oxidation (despite perfectly adequate redox potentials, Table 2, and excited state lifetimes, Fig. S14†).

Photocurrents and IQEs found here are lower than for some comparable systems with other catalysts.[7a,d,i] Brief analysis suggests the bottleneck is likely the 4th electron transfer from catalyst to dye: TAS measurements indicate a fast 1st ET, but give no information on later, less thermodynamically favourable ET events. Using 0.25 s^{-1} as a conservative estimate of **1**'s TOF (measured at ~0.1 to 0.82 s^{-1}),[2c,14b] and loadings of ~10 nmol cm^{-2}, steady state photocurrents of ~5 × 10^{-4} A might be expected – over ten times higher than those observed. In other words, **1** is operating well below its maximum TOF. The $Ru^{2+/3+}$ potentials of **P2** and **2** are very close to those of $[Ru(bpy)_3]^{2+}$,[23] and the driving force for the fourth ET from **1** to $[Ru(bpy)_3]^{2+}$ is small.[2c,n] Therefore, homogeneous systems need large $[Ru(bpy)_3]^{2+}$: **1** ratios (200 : 1) and generation of high Ru^{3+} : Ru^{2+} ratios to work efficiently.[11a] In our photoelectrodes, smaller excesses of sensitizer and a slow 4th ET prevent **1** from attaining its maximum TOF, leading to photo-bleaching and reduced light absorption – the situation is improved by **2**, which due to higher ε attains higher Ru^{3+} : Ru^{2+} ratios (*vide supra*), favouring the 4th ET. Further improvement may therefore come through (i) catalysts with lower overpotential or (ii) sensitizers with higher oxidation potentials[24] and extinction coefficients.

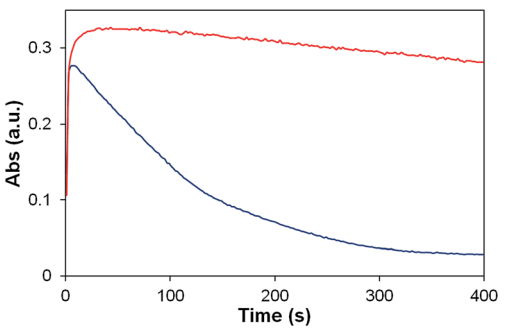

Fig. 9 UV-vis stopped flow experiment showing the self-decomposition of oxidized **P2** (red) and **2** (blue) at pH 1. Monitored at 670 nm (**P2**), 674 nm (**2**).

Stability of the sensitizers and photoelectrodes

Two processes – desorption of active species and oxidative damage to the sensitizers – cause the loss of activity seen in TiO_2-dye-**1** photoanodes. On short timescales, desorption seems to be more important: in our previous work[7i] similar losses of absorption (at 455 nm) occurred over 20 minutes whether films were subjected to photoelectrochemical conditions, or left in ambient light (pH 5.8 Na_2SiF_6/$NaHCO_3$). Other groups have found that illumination under *unbuffered* aqueous conditions promotes desorption of dye but does not cause noticeable photochemical degradation.[8a] Even so, a vital consideration for any sensitizer in light driven water oxidation is the stability of its oxidized (Ru^{3+}) state towards self-decomposition under turnover conditions. Oxidized Ru-polypyridyls are vulnerable, as nucleophilic attack of species such as H_2O, $[OH]^-$ and $[OOH]^-$ on the electron deficient pyridyl ring produces *O*-substituted species with oxidation potentials too low to continue driving water oxidation.[12] Therefore, dye stability limits TONs for POM WOCs in homogeneous light-driven water oxidation.[11] Below, we describe the loss of **1**, **P2** and **2** from the photoelectrodes at pH 5.8 and 7.2, and compare the oxidative stability of the two dyes, giving insight into the photoelectrochemical performance of the two photoanode systems.

Sensitizer and catalyst desorption studies. **P2** binds TiO_2 better below pH 5.[25] Therefore, pH > 5 buffers provide a driving force for dye desorption from TiO_2–**P2** and TiO_2–**2**. WOC **1** should also bind stronger at low pH: below the point-of-zero charge (pzc) of TiO_2 there is an electrostatic attraction between the positively charged surface and the ten negative charge of **1**. UV-vis monitored experiments have enabled us to investigate desorption of **1** and the sensitizers from TiO_2 films in our PEC conditions (pH 5.8 Na_2SiF_6/$NaHCO_3$ and pH 7.2 lutidine). While both the sensitizers and **1** have strong absorptions at *ca.* 455 nm, the differing pH dependencies of ε for the two species (for **1** ε_{455} is *ca.* 10 000 at pH >5, but 52 000 at pH 1)[2c] allow their contributions to be distinguished by acidification once desorbed into the buffer (ESI, Fig. S15–S18†). In all experiments, the desorbed species found in the soaking buffer solutions, plus the pH driven change in ε for **1** remaining on the TiO_2 surface, account for 70 to 95% of the observed absorbance loss of the films. The results, summarized in Table 5, demonstrate that, depending on pH, **2** mitigates loss of catalyst or dye. The evolution of absorbance loss over time (ESI, Fig, S19†) shows that in all cases losses are rapid initially, but are slowing by the end of the one hour experiment.

The films in Table 5 were assembled using constant soaking times and concentrations of **1**, so it is clear that the surface properties of TiO_2 are more important for catalyst loading than the charge of the dye. Metallating **2** only weakly influences the amount of catalyst bound during film assembly. This fits with previous findings that metal oxide pzc (TiO_2, SnO_2 or ZrO_2) critically influences **1** loading in **P2**-based triads.[7i] Upon soaking at pH 5.8, neither TiO_2–**P2**–**1** nor TiO_2–**2**–**1** leaches catalyst, but significant loss occurs at pH 7.2, which is reasonable given the pzc of TiO_2 (*ca.* 6) and the hydrophobicity of the THpA{**1**} salt. Importantly, these catalyst losses are cut dramatically (by 50%)

Table 5 Desorption of dye and catalyst **1** over 60 minutes from TiO_2 photoelectrodes in buffers used in this study

	pH 5.8 Na_2SiF_6/$NaHCO_3$/$NaClO_4$		pH 7.2 lutidine/$HClO_4$/$NaClO_4$			
Film	TiO_2–**P2–1**[a]	TiO_2–**2Na$_2$–1**[a]	TiO_2–**P2–1**	TiO_2–**2–1**	TiO_2–**2Na$_2$–1**	TiO_2–**2Mg$_2$–1**
Loading of dye (nmol cm^{-2})[a]	37	29	93	65	65	62
Loading of **1** (nmol cm^{-2})[a]	10	8	10	8	10	11
Dye : **1** ratio[b]	37 : 10	38 : 10	92 : 10	84 : 10	63 : 10	59 : 10
Dye lost to buffer[c]	69%	53%	22%	20%	22%	31%
1 lost to buffer[c]	0%	0%	30%	12%	15%	17%
Calcd. Loss film Abs_{455}[d]						
From: dye loss	39%	41%	17%	17%	17%	24%
Loss of **1**	0%	0%	7%	2%	3%	4%
pH effect on ε of **1**	29%	21%	11%	10%	12%	12%
Total calcd. loss film Abs_{455}	68%	62%	35%	29%	32%	40%
Actual loss film Abs_{455}[e]	76%	77%	48%	32%	40%	42%

[a] Loadings are based on flat surface areas, ignoring TiO_2 porosity. [b] Calculated from UV-vis absorbances of triad, dyad and parent TiO_2 film. [c] Calculated from absorbances of soaking solutions at 455 nm, at buffer pH and pH 1, and absorbances of the species on the TiO_2 film. [d] Predicted loss of film absorbance at 455 nm, after subtracting TiO_2 background, based on solution measurements. [e] Differences between calculated and actual film absorbance losses may be accounted for by unknowns such as the precise ε of the dyes on the TiO_2 surface, other pH driven changes in film absorbance, and inhomogeneities in the films.

for TiO_2–**2Na$_2$–1** *vs.* TiO_2–**P2–1**, showing that the crown derivative stabilizes binding of **1** to TiO_2 when pH > pzc. Interestingly, however, metallating with Mg^{2+} instead of Na^+ destabilizes the photoelectrodes – most likely by increasing the aqueous solubility of the dye – while the result for un-metallated **2** is similar (within likely experimental errors) to that of **2Na$_2$**. This suggests that the strengthened catalyst binding of **2** is as much a result of hydrophobic surface interactions that exclude water and buffer, as electrostatics.

Surprisingly, losses of the dyes do not follow the expected pH dependence and are much more severe at pH 5.8. We surmise that carbonate from the buffer competes with phosphonate for the TiO_2 surface, whilst lutidine does not. However, less **2** is lost than **P2** (53% *vs.* 69%), presumably because it associates more strongly with the catalyst that remains on the surface. Total % losses of absorbance from the **2** and **P2** photoanodes are similar though, which is explained by a lower dye contribution to the TiO_2–**P2–1** absorbance due to **P2**'s lower ε, and a higher loading of **1**. Thus, it appears that introducing a simple recognition group can help significantly in stabilizing the binding of polyoxometalates to ds-TiO_2.

Stopped-flow stability measurements on H$_2$2 and P2. Stopped-flow UV-vis measurements were carried out on oxidized **2** and **P2** at pH 1, by mixing with Ce^{4+} in H_2SO_4. The results (Fig. 9) indicate that **2** is substantially less stable than **P2** in its oxidized state, even at pH 1 having a half-life of only 100 s. Such stability differences increase with increasing pH. Indeed, in homogeneous catalysis, both **H$_2$2** and its tris-5-crown-phen analogue are incapable of driving water oxidation by **1** at pH 7.2. We therefore conclude that the weaker performance of TiO_2–**2Na$_2$–1** at pH 7.2, compared to pH 5.8, results partly from increased susceptibility of this dye to oxidative destruction. In fact, that TiO_2–**2** based photoanodes are able to oxidize water at all indicates that location on the TiO_2 surface has a remarkable stabilising effect on the dye.

Conclusions

We have confirmed that ds-TiO_2 treated with POM WOCs is able to oxidize water, at neutral pH and below. This is the first time that visible light-driven water oxidation has been demonstrated with a surface-immobilized POM species. Performance is higher at pH 5.8 than at pH 7.2, opposing the homogeneous trend: this is ascribed to dye stability, catalyst binding and electron transfer efficiency. It is also consistent with photoanode performance being limited by the 4th electron transfer rather than catalyst TOF_{max}, and indicates that optimum conditions for immobilized WOCs may vary from homogeneous use. We have also found that ds-TiO_2 itself oxidizes water, with high faradaic efficiency but substantially lower quantum efficiency than the catalysed systems. This suggests that care should be taken to run catalyst-free controls in related work, particularly if photocurrents are low (<10 μA).

This study also shows that increasing the extinction coefficient of the dye, across the range of 400 to 550 nm, is a very effective way to increase water oxidation photocurrents and quantum yields, and incorporating a simple supramolecular recognition motif (crown ether) stabilizes binding of POM WOCs at pH >TiO_2 pzc. However, it also indicates that oxidative stability of the dye under water oxidation conditions is a key consideration, and modifications which can reduce the stability of the dye to nucleophilic attack are best avoided. Adequate loadings and stable binding of the POM WOC can be achieved with unmodified dyes provided the operating pH remains below the pzc of the metal oxide substrate. It therefore appears that there are three profitable future directions for this work: (i) development of fast POM WOCs that operate efficiently below pH 6, with lower overpotential; (ii) producing strongly absorbing dyes, with high binding and oxidative stability and more positive redox potentials; and (iii) testing metal oxides with high points of zero charge, such as ZnO.

Lastly, we have shown that lutidine is a good, oxidation resistant organic buffer for near-neutral conditions and better tolerated by ds-TiO_2 than potentially surface-binding inorganic anions such as phosphate, borate and carbonate.

Experimental

General

Full details of materials, synthetic procedures, and instruments and methods used for primary structural characterization are available in the ESI.† UV-vis spectra were obtained using Agilent 8453 and Cary 60 spectrophotometers. Fluorescence spectra were acquired on a Perkin Elmer LS 55 fluorimeter. Electrochemical data (cyclic voltammetry) were obtained using BASi CV-50W and Autolab PGSTAT302N potentiostats in a three electrode configuration with Ag/AgCl reference, glassy carbon working and platinum counter electrodes. The electrolyte was 0.1 M $HClO_4$ in MeCN/H_2O (for $\mathbf{H_2 2}$), or 0.1 M NBu_4PF_6 (for $\mathbf{[Et_4 2][PF_6]_2}$). UV-visible stopped flow measurements were performed at 25 °C using a Hi-Tech KinetAsyst Stopped Flow SF-61SX2 equipped with a tungsten lamp and diode array detector (400–700 nm). The oxidant, $(NH_4)_4Ce(SO_4)_4 \cdot 2H_2O$ was dissolved in 0.1 M H_2SO_4 (0.4 M in $LiClO_4$) and the sensitizer was dissolved in 0.1 M H_2SO_4 alone.

Film preparation and characterization

Transparent TiO_2 films were prepared from colloidal suspensions by the doctor-blade technique, using Scotch tape to control area and thickness. The films were calcined at 400 °C for 90 minutes, soaked in acidic solutions of **P2** or $\mathbf{H_2 2}$ (0.2 mM in 0.1 M $HClO_{4(aq)}$) for 24 hours, and soaked 24 hours in 0.1 M $HClO_{4(aq)}$ to remove free or weakly-adsorbed dye molecules, before rinsing with water and drying in air. Metallation of TiO_2–**2** was achieved by soaking for 30 minutes in 0.1 M solutions of $NaClO_4$ or $Mg(ClO_4)_2$ in acetonitrile. TiO_2–**2–1** and TiO_2–$\mathbf{2M_2}$–**1** triads for ultrafast spectroscopy were prepared by soaking the dye-sensitized films in acetone solutions of TBA_7H_3[**1**] (0.15 to 1 mM) for 10 to 30 minutes, rinsing with acetone and air drying. For photoelectrochemistry, triads were instead prepared by soaking TiO_2–**P2** and TiO_2–$\mathbf{2Na_2}$ films in a 0.28 mM toluene solution of hydrophobic $THpA_{8.5}H_{1.5}$[**1**] for 5 minutes, rinsing with toluene and air drying. Dye-to-**1** ratios were estimated from UV-vis spectra (Fig. S4†) by using the extinction coefficients measured for $\mathbf{H_2 2}$ (19 100 M^{-1} cm^{-1} at 455 nm) and **P2** (11 700 M^{-1} cm^{-1}) to quantify the dye, and the estimated extinction coefficient of 32 000 M^{-1} cm^{-1} at 455 nm for **1** on the TiO_2 surface.[7i]

Computational details

Geometries and energetics of **P2**, $\mathbf{H_4 2}$, $\mathbf{H_4 2–Na_2}$ and $\mathbf{H_4 2–Mg_2}$ were calculated at their lower-lying electronic states, in aqueous solution with no geometry constraints. Vibrational analyses were performed to ensure that all converged structures are true minima. In these calculations we used the spin-unrestricted DFT method (the hybrid B3LYP functional)[26] in conjunction with the lanl2dz basis set with the associated Hay-Wadt ECPs[27] for Ru atoms, and the 6-31G(d) basis sets for all other atoms. Solvent effects were incorporated at the polarizable continuum model (PCM).[28] All calculations were carried out with the Gaussian 09 software package.[29]

Laser photophysical measurements

For ultrafast measurements, the femtosecond transient absorption spectrometer is based on a Ti:sapphire laser (coherent Legend, 800 nm, 150 fs, 3 mJ per pulse, 1 kHz repetition rate) and Helios spectrometer (Ultrafast Systems LLC). To probe the IR, a Clark IR optical parametric amplifier was used, generating two tunable near-IR pulses in the 1.1 to 2.5 μm range (signal and idler, respectively). Nanosecond to microsecond measurements were carried out in an EOS spectrometer (Ultrafast Systems LLC), with pump pulses generated from the above laser. Full details are in the ESI.†

Dye and catalyst desorption experiments

TiO_2–**P2–1**, TiO_2–**2–1** and TiO_2–$\mathbf{2M_2}$–**1** films (*ca.* 1.4 cm^2) were immersed in 3 mL of buffer solution. The films were removed after 2 seconds, and then 1, 5, 15, 30 and 60 minutes, and UV-vis spectra measured to assess the extent of desorption. UV-vis spectra of the soaking solutions were measured at the same intervals. At 60 minutes, the soaking solutions were acidified to *ca.* pH 1 by addition of a drop of concentrated H_2SO_4. As the 455 nm extinction coefficients of both dyes fall at low pH, while that of **1** dramatically increases, the change in absorbance can be used to assess relative contribution of the two species. See the ESI for further details (Fig. S15–S18†).

Photoelectrochemical measurements and oxygen detection

Photoelectrochemical measurements (chronoamperometry) were obtained in a two compartment electrochemical cell, with a flat fronted working compartment for the photoanode, under a constant stream of Ar gas. The potentiostat was an Autolab PGSTAT302N with bipotentiostat module, in four electrode configuration (WE1, WE2, reference and counter), and the light source a 455 nm LED (Osram) at 20 mW power output focused onto *ca.* 0.6 cm^2 with a fused silica lens. We used the generator/collector methods of Mallouk *et al.*,[21] with a platinized FTO detector film held *ca.* 1 mm from the working surface of the back-side illuminated photoanode, the sides of the assembly were sealed with wax and the bottom left open for ingress of buffer. The photoanode (generator) was set to an applied bias of 0 V *vs.* Ag/AgCl, and the detector to −0.5 V (pH 5.8) or −0.584 V (pH 7.2), and the photoanode exposed to the light for several 60 s transients. At pH 5.8 we used 38 mM Na_2SiF_6, adjusted to pH 5.8 using $NaHCO_3$ (final concentration *ca.* 80 mM), with $NaClO_4$ added for a total Na^+ concentration of 200 mM. At pH 7.2, we used 50 mM lutidine, adjusted to pH 7.2 with $HClO_4$, and 200 mM $NaClO_4$ supporting electrolyte. The collector efficiency was determined to be *ca.* 60% in both buffers, by calibrating with a platinised FTO generator film set to +1.1 or +1.2 V (depending on pH) *vs.* Ag/AgCl. For further details, including photographs and calibration methods, see the ESI (Fig. S20 and S21†).

Acknowledgements

We thank Dr Jie Song for help with synthesis of **P2**, Dr Kenneth Hardcastle for assisting with X-ray diffraction, and Dr Gregory G. Wildgoose for access to a bipotentiostat. Mass spectra for **[Et$_4$2](PF$_6$)$_2$** and [(Et$_4$dpbpy)$_2$Ru(5-crown-phen)](PF$_6$)$_2$ were obtained by the UK EPSRC National Mass Spectrometry facility in Swansea. Our work was funded by the U.S. Department of Energy, Office of Basic Energy Sciences, Solar Photochemistry Program (DE-FG02-07ER-15906) to C.L.H., T.L. and D.G.M.; the EU through a Marie Curie IOF to J.F. (POMHYDCAT, contract no. 254339), and by the University of East Anglia. X. X. thanks the China Scholarship Council and NSFC (#21376020) for financial support.

Notes and references

1 (*a*) R. A. Binstead, C. W. Chronister, J. Ni, C. M. Hartshorn and T. J. Meyer, *J. Am. Chem. Soc.*, 2000, **122**, 8464; (*b*) M. Yagi and M. Kaneko, *Chem. Rev.*, 2001, **101**, 21; (*c*) J. K. Hurst, *Coord. Chem. Rev.*, 2005, **249**, 313; (*d*) R. Zong and R. Thummel, *J. Am. Chem. Soc.*, 2005, **127**, 12802; (*e*) R. Eisenberg and H. B. Gray, *Inorg. Chem.*, 2008, **47**, 1697; (*f*) N. D. McDaniel, F. J. Coughlin, L. L. Tinker and S. Bernhard, *J. Am. Chem. Soc.*, 2008, **130**, 210; (*g*) R. Brimblecombe, G. F. Swiegers, G. C. Dismukes and L. Spiccia, *Angew. Chem., Int. Ed.*, 2008, **47**, 7335; (*h*) J. J. Concepcion, J. W. Jurss, M. K. Brennaman, P. G. Hoertz, A. O. T. Patrocinio, N. Y. M. Iha, J. L. Templeton and T. J. Meyer, *Acc. Chem. Res.*, 2009, **42**, 1954; (*i*) J. K. Hurst, J. L. Cape, A. E. Clark, S. Das and C. Qin, *Inorg. Chem.*, 2008, **47**, 1753; (*j*) T. A. Betley, Y. Surendranath, M. V. Childress, G. E. Alliger, R. Fu, C. C. Cummins and D. G. Nocera, *Philos. Trans. R. Soc., B*, 2008, **363**, 1293; (*k*) J. T. Muckerman, D. E. Polyansky, T. Wada, K. Tanaka and E. Fujita, *Inorg. Chem.*, 2008, **47**, 1787; (*l*) X. Sala, I. Romero, M. Rodríguez, L. Escriche and A. Llobet, *Angew. Chem., Int. Ed.*, 2009, **48**, 2842; (*m*) R. Nakamura and H. Frei, *J. Am. Chem. Soc.*, 2006, **128**, 10668; (*n*) F. Jiao and H. Frei, *Angew. Chem., Int. Ed.*, 2009, **48**, 1841; (*o*) J. F. Hull, D. Balcells, J. D. Blakemore, C. D. Incarvito, O. Eisenstein, G. W. Brudvig and R. H. Crabtree, *J. Am. Chem. Soc.*, 2009, **131**, 8730; (*p*) L. Duan, Y. Xu, M. Gorlov, L. Tong, S. Andersson and L. Sun, *Chem.–Eur. J.*, 2010, **16**, 4659; (*q*) S. Masaoka and K. Sakai, *Chem. Lett.*, 2009, **38**, 182; (*r*) L. Duan, F. Bozoglian, S. Mandal, B. Stewart, T. Privalov, A. Llobet and L. Sun, *Nat. Chem.*, 2012, **4**, 418; (*s*) Z. Chen and T. J. Meyer, *Angew. Chem., Int. Ed.*, 2013, **52**, 700.

2 (*a*) Y. V. Geletii, B. Botar, P. Kögerler, D. A. Hillesheim, D. G. Musaev and C. L. Hill, *Angew. Chem., Int. Ed.*, 2008, **47**, 3896; (*b*) A. Sartorel, M. Carraro, G. Scorrano, R. D. Zorzi, S. Geremia, N. D. McDaniel, S. Bernhard and M. Bonchio, *J. Am. Chem. Soc.*, 2008, **130**, 5006; (*c*) Y. V. Geletii, C. Besson, Y. Hou, Q. Yin, D. G. Musaev, D. Quinonero, R. Cao, K. I. Hardcastle, A. Proust, P. Kögerler and C. L. Hill, *J. Am. Chem. Soc.*, 2009, **131**, 17360; (*d*) A. E. Kuznetsov, Y. V. Geletii, C. L. Hill, K. Morokuma and D. G. Musaev, *J. Am. Chem. Soc.*, 2009, **131**, 6844; (*e*) A. Sartorel, P. Miro, E. Salvadori, S. Romain, M. Carraro, G. Scorrano, M. D. Valentin, A. Llobet, C. Bo and M. Bonchio, *J. Am. Chem. Soc.*, 2009, **131**, 16051; (*f*) C. Besson, Z. Huang, Y. V. Geletii, S. Lense, K. I. Hardcastle, D. G. Musaev, T. Lian, A. Proust and C. L. Hill, *Chem. Commun.*, 2010, **46**, 2784; (*g*) Q. Yin, J. M. Tan, C. Besson, Y. V. Geletii, D. G. Musaev, A. E. Kuznetsov, Z. Luo, K. I. Hardcastle and C. L. Hill, *Science*, 2010, **328**, 342; (*h*) R. Cao, H. Ma, Y. V. Geletii, K. I. Hardcastle and C. L. Hill, *Inorg. Chem.*, 2009, **48**, 5596; (*i*) F. Song, Y. Ding, B. Ma, C. Wang, Q. Wang, X. Du, S. Fu and J. Song, *Energy Environ. Sci.*, 2013, **6**, 1170; (*j*) H. Lv, J. Song, Y. V. Geletii, J. W. Vickers, J. M. Sumliner, D. G. Musaev, P. Kögerler, P. F. Zhuk, J. Basca, G. Zhu and C. L. Hill, *J. Am. Chem. Soc.*, 2014, **136**, 9268; (*k*) S. Goberna-Ferrón, L. Vigara, J. Soriano-López and J. R. Galán-Mascarós, *Inorg. Chem.*, 2012, **51**, 11707; (*l*) H. Lv, Y. V. Geletii, C. Zhao, J. W. Vickers, G. Zhu, Z. Luo, J. Song, T. Lian, D. G. Musaev and C. L. Hill, *Chem. Soc. Rev.*, 2012, **41**, 7572; (*m*) R. Al-Oweini, A. Sartorel, B. S. Bassil, M. Natali, S. Berardi, F. Scandola, U. Kortz and M. Bonchio, *Angew. Chem., Int. Ed.*, 2014, **53**, 11182; (*n*) Y. Liu, S.-X. Guo, A. M. Bond, J. Zhang, Y. V. Geletii and C. L. Hill, *Inorg. Chem.*, 2013, **52**, 11986.

3 (*a*) W. J. Youngblood, S.-H. A. Lee, K. Maeda and T. E. Mallouk, *Acc. Chem. Res.*, 2009, **42**, 1966; (*b*) L. Duan, L. Tong, Y. Xu and L. Sun, *Energy Environ. Sci.*, 2011, **4**, 3296; (*c*) W. Song, Z. Chen, C. R. K. Glasson, K. Hanson, H. Luo, M. R. Norris, D. L. Ashford, J. J. Concepcion, M. K. Brennaman and T. J. Meyer, *ChemPhysChem*, 2012, **13**, 2882; (*d*) D. G. Nocera, *Acc. Chem. Res.*, 2012, **45**, 767.

4 (*a*) S. Anderson, E. C. Constable, M. P. Dare-Edwards, J. B. Goodenough, A. Hamnett, K. R. Seddon and R. D. Wright, *Nature*, 1979, **280**, 571; (*b*) M. P. Dare-Edwards, J. B. Goodenough, A. Hamnett, K. R. Seddon and R. D. Wright, *Faraday Discuss. Chem. Soc.*, 1980, **70**, 285; (*c*) R. Memming and F. Schröppel, *Chem. Phys. Lett.*, 1979, **62**, 207; (*d*) R. Memming, F. Schröppel and U. Bringmann, *J. Electroanal. Chem.*, 1979, **100**, 307.

5 A. Juris and V. Balzani, *Coord. Chem. Rev.*, 1988, **84**, 85.

6 A. Hagfeldt, G. Boschloo, L. Sun, L. Kloo and H. Pettersson, *Chem. Rev.*, 2010, **110**, 6595.

7 (*a*) W. J. Youngblood, S.-H. A. Lee, Y. Kobayashi, E. A. Hernandez-Pagan, P. G. Hoertz, T. A. Moore, A. L. Moore, D. Gust and T. E. Mallouk, *J. Am. Chem. Soc.*, 2009, **131**, 926; (*b*) R. Brimblecombe, A. Koo, G. C. Dismukes, G. F. Swiegers and L. Spiccia, *J. Am. Chem. Soc.*, 2010, **132**, 2892; (*c*) L. Li, L. Duan, Y. Xu, M. Gorlov, A. Hagfeldt and L. Sun, *Chem. Commun.*, 2010, **46**, 7307; (*d*) Y. Zhao, J. R. Swierk, J. D. Megiatto, B. Sherman, W. J. Youngblood, D. Qin, D. M. Lentz, A. L. Moore, T. A. Moore, D. Gust and T. E. Mallouk, *Proc. Natl. Acad. Sci. U. S. A.*, 2012, **109**, 15612; (*e*) G. F. Moore, J. D. Blakemore, R. L. Milot, J. F. Hull, H. Song, L. Cai, C. A. Schmuttenmaer, R. H. Crabtree and G. W. Brudvig,

Energy Environ. Sci., 2011, **4**, 2389; (*f*) W. Song, C. R. K. Glasson, H. Luo, K. Hanson, M. K. Brennaman, J. J. Concepcion and T. J. Meyer, *J. Phys. Chem. C*, 2011, **115**, 7081; (*g*) W. Song, C. R. K. Glasson, H. Luo, K. Hanson, M. K. Brennaman, J. J. Concepcion and T. J. Meyer, *J. Phys. Chem. Lett.*, 2011, **2**, 1808; (*h*) G. Li, E. M. Sproviero, W. R. McNamara, R. C. Snoeberger, R. H. Crabtree, G. W. Brudvig and V. S. Batista, *J. Phys. Chem. B*, 2010, **114**, 14214; (*i*) X. Xiang, J. Fielden, W. Rodríguez-Córdoba, Z. Huang, N. Zhang, Z. Luo, D. G. Musaev, T. Lian and C. L. Hill, *J. Phys. Chem. C*, 2013, **117**, 918; (*j*) Y. Gao, X. Ding, J. Liu, L. Wang, Z. Lu, L. Li and L. Sun, *J. Am. Chem. Soc.*, 2013, **135**, 4219; (*k*) D. L. Ashford, A. M. Lapides, A. K. Vannucci, K. Hanson, D. A. Torelli, D. P. Harrison, J. L. Templeton and T. J. Meyer, *J. Am. Chem. Soc.*, 2014, **136**, 6578; (*l*) L. Alibabaei, M. K. Brennaman, M. R. Norris, B. Kalanyan, W. Song, M. D. Losego, J. J. Concepcion, R. A. Binstead, G. N. Parsons and T. J. Meyer, *Proc. Natl. Acad. Sci. U. S. A.*, 2013, **110**, 20008.

8 (*a*) K. Hanson, M. K. Brennaman, H. Luo, C. R. K. Glasson, J. J. Concepcion, W. Song and T. J. Meyer, *ACS Appl. Mater. Interfaces*, 2012, **4**, 1462; (*b*) A. K. Vannucci, L. Alibabaei, M. D. Losego, J. J. Concepcion, B. Kalanyan, G. N. Parsons and T. J. Meyer, *Proc. Natl. Acad. Sci. U. S. A.*, 2013, **110**, 20918; (*c*) K.-R. Wee, M. K. Brennaman, L. Alibabaei, B. H. Farnum, B. Sherman, A. M. Lapides and T. J. Meyer, *J. Am. Chem. Soc.*, 2014, **136**, 13514; (*d*) K. Hanson, M. D. Losego, B. Kalanyan, D. L. Ashford, G. N. Parsons and T. J. Meyer, *Chem. Mater.*, 2013, **25**, 3; (*e*) A. M. Lapides, D. L. Ashford, K. Hanson, D. A. Torelli, J. L. Templeton and T. J. Meyer, *J. Am. Chem. Soc.*, 2013, **135**, 15450.

9 (*a*) M. Orlandi, R. A. Sartorel, M. Carraro, G. Scorrano, M. Bonchio and F. Scandola, *Chem. Commun.*, 2010, **46**, 3152; (*b*) Z. Huang, Y. V. Geletii, D. G. Musaev, C. L. Hill and T. Lian, *Ind. Eng. Chem. Res.*, 2012, **51**, 11850.

10 (*a*) S.-X. Guo, Y. Liu, C.-Y. Lee, A. M. Bond, J. Zhang, Y. V. Geletii and C. L. Hill, *Energy Environ. Sci.*, 2013, **6**, 2654; (*b*) S.-X. Guo, C.-Y. Lee, J. Zhang, A. M. Bond, Y. V. Geletii and C. L. Hill, *Inorg. Chem.*, 2014, **53**, 7561; (*c*) N. Anwar, A. Sartorel, M. Yaqub, K. Wearen, F. Laffir, G. Armstrong, C. Dickinson, M. Bonchio and T. McCormac, *ACS Appl. Mater. Interfaces*, 2012, **6**, 8022; (*d*) J. Soriano-López, S. Goberna-Ferrón, L. Vigara, J. J. Carbó, J. M. Poblet and J. R. Galán-Mascarós, *Inorg. Chem.*, 2013, **52**, 4753; (*e*) J. Wu, L. Liao, W. Yan, Y. Xue, Y. Sun, X. Yan, Y. Chen and Y. Xi, *ChemSusChem*, 2012, **5**, 1207; (*f*) F. M. Toma, A. Sartorel, M. Iurlo, M. Carraro, P. Parisse, C. Maccato, S. Rapino, B. R. Gonzalez, H. Amenitsch, T. Da Ros, L. Casalis, A. Goldoni, M. Marcaccio, G. Scorrano, G. Scoles, F. Paolucci, M. Prato and M. Bonchio, *Nat. Chem.*, 2010, **2**, 826.

11 (*a*) Y. V. Geletii, Z. Huang, Y. Hou, D. G. Musaev, T. Lian and C. L. Hill, *J. Am. Chem. Soc.*, 2009, **131**, 7522; (*b*) F. Puntoriero, G. L. Ganga, A. Sartorel, M. Carraro, G. Scorrano, M. Bonchio and S. Campagna, *Chem. Commun.*, 2010, **46**, 4725; (*c*) Z. Huang, Z. Luo, Y. V. Geletii, J. W. Vickers, Q. Yin, D. Wu, Y. Hou, Y. Ding, J. Song, D. G. Musaev, C. L. Hill and T. Lian, *J. Am. Chem.Soc.*, 2011, **133**, 2068; (*d*) J. W. Vickers, H. Lv, J. M. Sumliner, G. Zhu, Z. Luo, D. G. Musaev, Y. V. Geletii and C. L. Hill, *J. Am. Chem. Soc.*, 2013, **135**, 14110; (*e*) H. Lv, J. A. Rudd, P. F. Zhuk, J. Y. Lee, E. C. Constable, C. E. Housecroft, C. L. Hill, D. G. Musaev and Y. V. Geletii, *RSC Adv.*, 2013, **3**, 20647; (*f*) J. M. Sumliner, H. Lv, J. Fielden, Y. V. Geletii and C. L. Hill, *Eur. J. Inorg. Chem.*, 2014, 635; (*g*) G. Zhu, E. Glass, C. Zhao, H. Lv, J. W. Vickers, Y. V. Geletii, D. G. Musaev, J. Song and C. L. Hill, *Dalton Trans.*, 2012, 13043.

12 (*a*) C. Creutz and N. Sutin, *Proc. Natl. Acad. Sci. U. S. A.*, 1975, **72**, 2858; (*b*) P. K. Ghosh, B. S. Brunschwig, M. C. Chou, C. Creutz and N. Sutin, *J. Am. Chem. Soc.*, 1984, **106**, 4772.

13 (*a*) A. Proust, B. Matt, R. Villanneau, G. Guillemot, P. Gouzerh and G. Izzet, *Chem. Soc. Rev.*, 2012, **41**, 7605; (*b*) A. Dolbecq, E. Dumas, C. R. Mayer and P. Mialane, *Chem. Rev.*, 2010, **110**, 6009.

14 (*a*) V. W.-W. Yam, V. W.-M. Lee, F. Ke and K.-W. M. Siu, *Inorg. Chem.*, 1997, **36**, 2124; (*b*) C. R. Rice, A. Guerrero, Z. R. Bell, R. L. Paul, G. R. Motson, J. C. Jeffery and M. D. Ward, *New J. Chem.*, 2001, **25**, 185.

15 J. Ettedgui, Y. Diskin-Posner, L. Weiner and R. Neumann, *J. Am. Chem. Soc.*, 2011, **133**, 188.

16 P. U. Maheswari, V. Rajendran, M. Palaniandavar, R. Thomas and G. U. Kulkarni, *Inorg. Chim. Acta*, 2006, **359**, 4601.

17 Selected examples: (*a*) J. B. Asbury, R. J. Ellingson, H. N. Ghosh, S. Ferrere, A. J. Nozik and T. Lian, *J. Phys. Chem. B*, 1999, **103**, 3110; (*b*) J. B. Asbury, Y. Q. Wang and T. Lian, *J. Phys. Chem. B*, 1999, **103**, 6643; (*c*) T. A. Heimer and E. J. Heilweil, *J. Phys. Chem. B*, 1997, **101**, 10990; (*d*) Y. Trachibana, S. A. Haque, I. P. Mercer, J. R. Durrant and D. R. Klug, *J. Phys. Chem. B*, 2000, **104**, 1198; (*e*) R. C. Snoeberger, K. J. Young, J. Tang, L. J. Allen, R. H. Crabtree, G. W. Brudvig, P. Coppens, V. S. Batista and J. B. Benedict, *J. Am. Chem. Soc.*, 2012, **134**, 8911; (*f*) J. Huang, D. Stockwell, A. Boulesbaa, J. Guo and T. Lian, *J. Phys. Chem. C*, 2008, **112**, 5203; (*g*) D. Stockwell, Y. Yang, J. Huang, C. Anfuso, Z. Huang and T. Lian, *J. Phys. Chem. C*, 2010, **114**, 6560; (*h*) K. Hanson, M. K. Brennaman, A. Ito, H. Luo, W. Song, K. A. Parker, R. Ghosh, M. R. Norris, C. R. K. Glasson, J. J. Concepcion, R. Lopez and T. J. Meyer, *J. Phys. Chem. C*, 2012, **116**, 14837; (*i*) R. Ernstorfer, L. Gundlach, S. Felber, W. Storck, R. Eichberger and F. Willig, *J. Phys. Chem. B*, 2006, **110**, 25383.

18 J. M. Gardner, M. Beyler, M. Karnahl, S. Tschierlei, S. Ott and L. Hammarström, *J. Am. Chem. Soc.*, 2012, **134**, 19322.

19 M. Natali, M. Orlandi, S. Berardi, S. Campagna, M. Bonchio, A. Sartorel and F. Scandola, *Inorg. Chem.*, 2012, **51**, 7324.

20 (*a*) T. E. Keyes, E. Gicquel, L. Guerin, V. M. Hultgren, A. M. Bond and A. G. Wedd, *Inorg. Chem.*, 2003, **42**, 7897; (*b*) M. K. Seery, L. Guerin, R. J. Forster, E. Gicquel, V. M. Hultgren, A. M. Bond, A. G. Wedd and T. E. Keyes,

J. Phys. Chem. A, 2004, **108**, 7399; (*c*) N. Fay, V. M. Hultgren, A. G. Wedd, T. E. Keyes, R. J. Forster, D. Leane and A. M. Bond, *Dalton Trans.*, 2006, 4218; (*d*) M. K. Seery, N. Fay, T. McCormac, E. Dempsey, R. J. Forster and T. E. Keyes, *Phys. Chem. Chem. Phys.*, 2005, **7**, 3426.

21 S.-H. A. Lee, Y. Zhao, E. A. Hernandez-Pagan, L. Blasdel, W. J. Youngblood and T. E. Mallouk, *Faraday Discuss.*, 2012, **155**, 165.

22 D. Duonghong, E. Borgarello and M. Grätzel, *J. Am. Chem. Soc.*, 1981, **103**, 4685.

23 A. Juris and V. Balzani, *Coord. Chem. Rev.*, 1988, **84**, 85.

24 D. L. Ashford, M. K. Brennaman, R. J. Brown, S. Keinan, J. J. Concepcion, J. M. Papanikolas, J. L. Templeton and T. J. Meyer, *Inorg. Chem.*, 2015, **54**, 460.

25 H. Park, E. Bae, J.-J. Lee, J. Park and W. Choi, *J. Phys. Chem. B*, 2006, **110**, 8740.

26 (*a*) A. D. Becke, *Phys. Rev. A*, 1988, **38**, 3098; (*b*) C. Lee, W. Yang and R. G. Parr, *Phys. Rev. B: Condens. Matter Mater. Phys.*, 1988, **37**, 785; (*c*) A. D. Becke, *J. Chem. Phys.*, 1993, **98**, 1372.

27 For ECP see: (*a*) P. J. Hay and W. R. Wadt, *J. Chem. Phys.*, 1985, **82**, 299; (*b*) P. J. Hay and W. R. Wadt, *J. Chem. Phys.*, 1985, **82**, 284; (*c*) W. R. Wadt and P. J. Hay, *J. Chem. Phys.*, 1997, **107**, 3032.

28 For PCM method see: (*a*) J. Tomasi and M. Persico, *Chem. Rev.*, 1994, **94**, 2027, and (*b*) R. Cammi and J. Tomasi, *J. Comput. Chem.*, 1995, **16**, 1449.

29 M. J. Frisch, G. W. Trucks, H. B. Schlegel, G. E. Scuseria, M. A. Robb, J. R. Cheeseman, G. Scalmani, V. Barone, B. Mennucci, G. A. Petersson, H. Nakatsuji, M. Caricato, X. Li, H. P. Hratchian, A. F. Izmaylov, J. Bloino, G. Zheng, J. L. Sonnenberg, M. Hada, M. Ehara, K. Toyota, R. Fukuda, J. Hasegawa, M. Ishida, T. Nakajima, Y. Honda, O. Kitao, H. Nakai, T. Vreven, J. A. Montgomery Jr, J. E. Peralta, F. Ogliaro, M. Bearpark, J. J. Heyd, E. Brothers, K. N. Kudin, V. N. Staroverov, R. Kobayashi, J. Normand, K. Raghavachari, A. Rendell, J. C. Burant, S. S. Iyengar, J. Tomasi, M. Cossi, N. Rega, J. M. Millam, M. Klene, J. E. Knox, J. B. Cross, V. Bakken, C. Adamo, J. Jaramillo, R. Gomperts, R. E. Stratmann, O. Yazyev, A. J. Austin, R. Cammi, C. Pomelli, J. W. Ochterski, R. L. Martin, K. Morokuma, V. G. Zakrzewski, G. A. Voth, P. Salvador, J. J. Dannenberg, S. Dapprich, A. D. Daniels, Ö. Farkas, J. B. Foresman, J. V. Ortiz, J. Cioslowski and D. J. Fox, *Gaussian 09, Revision D.01*, Gaussian, Inc., Wallingford CT, 2009.